XX IMEKO World Congress
Metrology for Green Growth
September 9–14, 2012, Busan, Republic of Korea

ESTIMATION OF IMAGE MOTION FOR WIDE FIELD TELESCOPE UNDER WIND LOADS

Il Kweon Moon[1], Sangon Lee[1], Juhee Lim[1,2], Joung Ung Lee[3], Ho-Soon Yang[1], and Yun Woo Lee[1]

[1] Korea Research Institute of Standards and Science, Daejon, S. Korea,
267 Gajeong-Ro, Yuseong-Gu, Daejeon, 305-340
[2] School of Space Research, Kyung Hee University, Yongin, S. Korea,
1732 Deogyeong-daero, Giheung-gu, Yongin-si, Gyeonggi-do, 446-701
[3] Department of Laser and Optical Information Engineering, Cheongju University, Choengju, S. Korea
Daeseong-Ro, Sangdang-Gu, Cheongju, Chungbuk, 360-704

ABSTRACT: To evaluate opto-mechanical performances under a certain level of windy environment, an estimation of the image motion is useful for a wide field telescope optical system. The wide field telescope is a Cassegrain telescope composed of two hyperbolic mirrors, a 0.5 m primary mirror and a 0.2 m secondary mirror, and correction lenses and then covers a 2° field of view. We performed the image motion analyses from the dynamic response based on the line of sight (LOS) sensitivity equations, which had been derived from the optical design program Code V, integrated in the finite element models by using NX NASTRAN.

Keywords: Wide field telescope, FEA, Image motion, Dynamic response

1. INTRODUCTION

A wide field telescope will be installed on the site of Mongolia, South Africa, and Turkey due to the clear and wide sky view. Those sites are naturally under a certain level of environmental conditions such as temperature, wind, humidity, local vibration, and earthquake. Those environmental conditions affect the opto-mechanical performances of the wide field telescope with structure thermal expansion or displacement due to static and dynamic loads. The transformed structures make displacement of an image motion at the image plane. Especially wind of the site introduces the image motion produced by the dynamic responses of each optical component. To estimate the image motion, the dynamic response of the wide field telescope is calculated under real measured wind data at Mongolia site. As a design goal for the wide field telescope, the image motion limit of the structure should be less than 1 pixel size of CCD, 9 ㎛, on the image plane [1]. Since the image motion is sensitive to the relative motion of the optical elements, the telescope structure was optimized with mirrors, lenses, and their mounting system under dynamic loads.

The optical system of the wide field telescope is constructed with two hyperbolic mirrors, five lenses, a filter, and a window, which covers a 2° field of view for wavelength from 365 nm to 900 nm. The primary mirror is a Zerodur hyperbolic mirror with a 500 mm diameter clear aperture and has a 140 mm diameter central hole. The aperture of the primary mirror functions as the stop of telescope. The secondary mirror is a Zerodur hyperbolic convex mirror with 200 mm diameter. A novel and unique optical design was conducted to obtain the long working distance from the last lens to focal plane. This optical design was composed of five lenses as the aberration corrector and the focus compensator. The filter and the window were mounted on the same structure on the CCD camera module. The optical layout of the wide field telescope is shown in Figure 1.

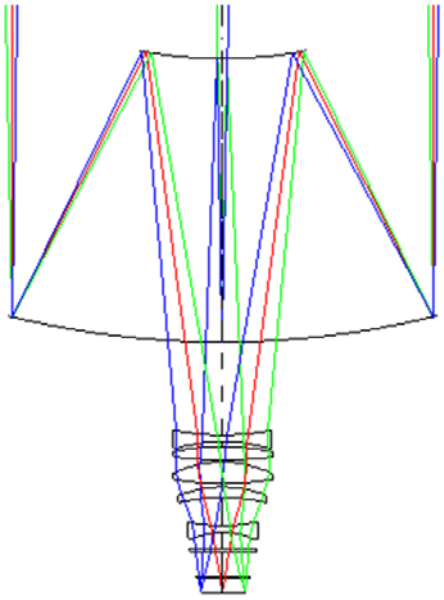

Figure 1. Optical layout of wide field telescope

The image motion by the acoustic vibration due to wind needs to be analyzed in the dynamic response mode. To calculate the image motion analyses, a specialized modeling

technique may be required. The image motion based on a two-mirror system was estimated by using the simple geometrical relationship introduced by several large telescope projects [2-4]. The line of sight, LOS, which connects with each optical element to the image plane, is a useful method for estimating the image motions of the optical systems. The physical point, i.e. nodal point of the optical elements should be composed on the finite element model to obtain the nodal dynamic response, namely image motion. The structural deformation is occurred due to the dynamic loads on the telescope, and then the physical image point, integrated in the finite element analysis model, is moved according to the LOS of nodal points on the finite element model. The result of the dynamic response analysis in accordance with time history is expressed in a time series.

2. MODELING OF IMAGE MOTION WITH SENSITIVITY AND FINITE ELEMENT ANALYSIS

The wide field telescope structure consists of the primary mirror (M1) assembly, the secondary mirror (M2) assembly, the yoke interface, the assembly of lenses, and the CCD camera part in order. The components of the M1 assembly are the inner barrel and a group (G1) of the primary mirror, and its M1 support system is composed of three axial supporters and three lateral supports connected to the inner barrel. The M2 assembly includes the upper barrel and a group (G2) of the secondary mirror with the M2 mounting system, alignment system, and support spiders. The components of the yoke interface are the outer wall and two side walls on the x-axis, each of side wall has a hole to combine the yoke on the same height as the center of the telescope of gravity along the z-axis. In the current design and development process, the yoke and its interface are rigidly connected, and five lenses, L1, L2, L3, L4, and L5, are mounted on one lens barrel. The components of the CCD module are the CCD cover, a group of filters, a window, a detecting system (chopper, shutter, and field derotator), and a CCD (G3). The material for telescope structure was chosen with design considerations of stiffness, lightweight, thermal stability, ease of fabrication, dynamic stability, and cost. Under these considerations, aluminum and invar were mainly used to fulfill the opto-mechanical performance criteria.

By using the program NX NASTRAN, we established the high-fidelity finite element to analyze the image motion of the telescope precisely. G1, G2, five lenses, and G3 are modeled as lumped mass elements at the center of gravity of the each element and assumed to be rigidly connected to the inner barrel, the upper barrel, the base of the inner barrel, and CCD cover, respectively. The finite element model for the current analysis is shown in Figure 2.

For the practical approach to the image motion study, an optical sensitivity analyzed by the optical design program Code V was taken for the LOS. The sensitivity for this paper is associated with only the image motion on the image plane related with rigid body motions of each optical element, not to the optical performance evaluation. The sensitivity of the wide field telescope on the image plane was calculated, and the results are expressed in Equation (1).

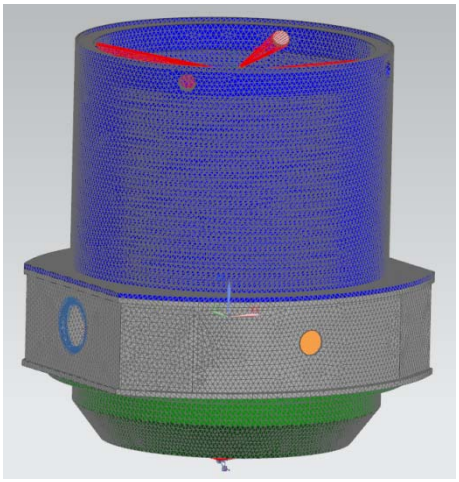

Figure 2. Finite element model of wide field telescope for the image motion analyses

$$
\begin{aligned}
T^{x}_{image} &= 2.908T^{x}_{G1} + 3.011R^{\beta}_{G1} - 2.115T^{x}_{G2} - 1.057R^{\beta}_{G2} \\
&- 0.789T^{x}_{L1} + 0.007R^{\beta}_{L1} + 0.469T^{x}_{L2} - 0.008R^{\beta}_{L2} + 0.886T^{x}_{L3} \\
&- 0.015R^{\beta}_{L3} + 0.226T^{x}_{L4} - 0.004R^{\beta}_{L4} - 0.570T^{x}_{L5} - 0.006R^{\beta}_{L5} \\
&- T^{x}_{G3} - 0.002R^{\beta}_{G3}
\end{aligned}
\tag{1}
$$

$$
\begin{aligned}
T^{y}_{image} &= 2.908T^{y}_{G1} - 3.006R^{\alpha}_{G1} - 2.115T^{y}_{G2} + 1.057R^{\alpha}_{G2} \\
&- 0.789T^{y}_{L1} - 0.007R^{\alpha}_{L1} + 0.469T^{y}_{L2} + 0.008R^{\alpha}_{L2} + 0.886T^{y}_{L3} \\
&+ 0.015R^{\alpha}_{L3} + 0.226T^{y}_{L4} + 0.004R^{\alpha}_{L4} - 0.570T^{y}_{L5} + 0.006R^{\alpha}_{L5} \\
&- T^{y}_{G3} + 0.002R^{\alpha}_{G3}
\end{aligned}
$$

In Eq. (1), the capital R and T represent the tilt and decenter, which are applicable to the G1, G2, five lenses, and G3. The superscript x and y express the coordinates. A set of the prescribed displacements referred to as constraints, for this case the image motion, provides a convenient boundary condition to solve the problem [5].

The constraint equations are related to the nodal degrees of freedom to the displacement of one or more other freedoms. A typical form is similar to Eq. (1), and the left-hand sides of the constraints, the displacement of the image on the image plane, may be referred to as the slave or dependent degrees of freedom because the displacement is completely defined by the right-hand sides of the equations expressed by the tilt and decenter of G1, G2, five lenses, and G3. The multi-point constraints (MPCs) were constructed for the image translations of the x-axis and the y-axis by using the finite element analysis program NX NASTRAN with Eq. (1) to calculate the image motion. The other constraint for the current analyses is the rigidly fixed constraint on the yoke interface surface between the barrel and the yoke.

3. IMAGE MOTION UNDER WIND LOADS

Many of the latest large telescope projects have performed and reported some level of wind buffeting analysis [6-8]. In these references, they used a load of the wind force obtained from a measurement of the wind velocity at the observatory or scaled from it. The measured wind velocity is sometimes too fast to sustain a stable image

motion. For the safety of the telescope, we had to clarify whether we could observe the object under a certain level of wind speed. For these reasons we used real measured wind data from the site in Mongolia.

For the excitation forcing function, data of the wind velocity were recorded at 8 AM in the morning, at 4 PM in the afternoon, and at midnight for 1 year as shown Figures 3 (a), (b), and (c), respectively. The calculated excitation functions at 8 AM, 4 PM, and midnight were determined on the finite element model by using NX NASTRAN. A parametric study was conducted, and it yields an optimal performance under dynamic performances of the secondary mirror because the secondary mirror (M2) assembly is regarded as the weakest part of the wide field telescope structure. To predict the upper limit for the worst case, we applied the dynamic load to the vertex of the secondary mirror.

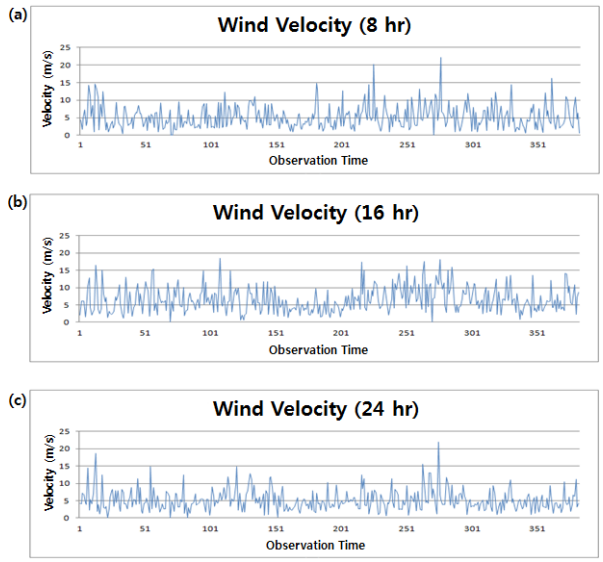

(a) profile of wind velocity recorded at 8 hour in the morning,

(b) profile of wind velocity recorded at 16 hour in the afternoon, and

(c) profile of wind velocity recorded at 24 hour at midnight.

Figure 3. Profile of wind velocity recorded for 1 year

From the excitation force at 8 hours, 16 hours, and 24 hours, the LOS along the x-axis and y-axis of the image motion responses were calculated. As one of the sample case of the x-axis image motion response, the excitation force at 8 hours is calculated and shown as Figure 4. The responses of the excitation force along the x-axis, y-axis, and z-axis are shown in Figures 4 (a), (b), and (c), respectively. The magnitudes of the image motions from the excitation force along the x-axis, y-axis, and z-axis are 0.232 ㎛, 0.00007 ㎛, and 0.0003 ㎛ with RMS (root mean square) values of 32 ㎚, 0.0092 ㎚, and 0.0398 ㎚, respectively.

Figure 5 shows the sample case of the y-axis image motion response to the excitation force at 8 hour. The responses of the excitation force along the x-axis, y-axis, and z-axis are shown in Figures 5 (a), (b), and (c), respectively. The maximum magnitudes of the motions from the excitation force along the x-axis, y-axis, and z-axis are 0.0000693 ㎛, 0.607 ㎛, and 0.00161 ㎛ with RMS values of 0.0106 ㎚, 105 ㎚, and 0.434 ㎚, respectively.

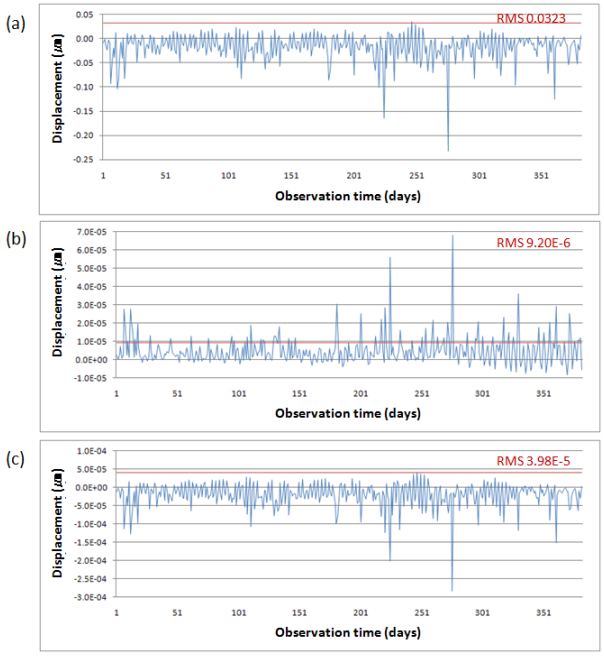

(a) response of image motion to excitation along X,

(b) response of image motion to excitation along Y, and

(c) response of image motion to excitation along Z.

Figure 4. X-axis image motion response to wind at 8 hour

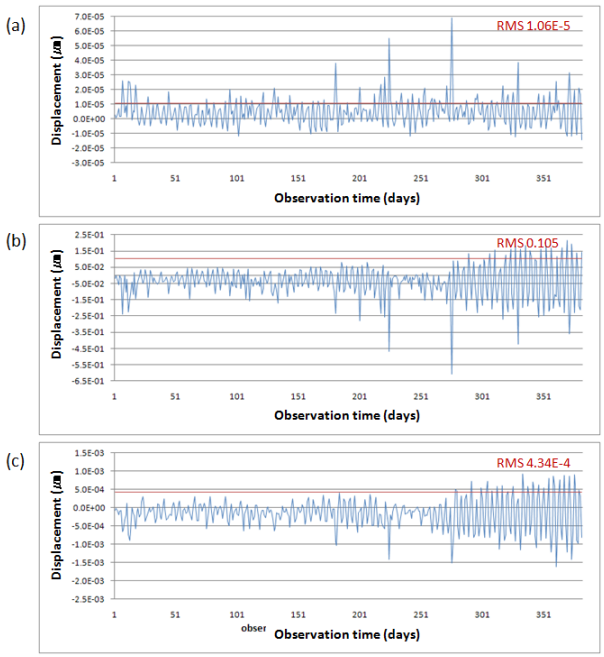

(a) response of image motion to excitation along X,

(b) response of image motion to excitation along Y, and

(c) response of image motion to excitation along Z.

Figure 5. Y-axis image motion response to wind at 8 hour

Table 1. Results of the image motion responses

Image motion	Excitation force	Hour	Min	Max	Magnitude	Average	RMS
X	x	8	-0.232	0.035	0.232	-0.017	0.032
		16	-0.153	0.043	0.153	-0.025	0.042
		24	-0.241	0.030	0.241	-0.016	0.030
	y	8	-8.13E-06	6.83E-05	6.83E-05	5.03E-06	9.20E-06
		16	-7.83E-06	4.68E-05	4.68E-05	7.35E-06	1.17E-06
		24	-4.91E-06	6.34E-05	6.34E-05	4.68E-06	8.32E-06
	z	8	-2.83E-04	4.06E-05	2.83E-04	-2.09E-05	3.98E-05
		16	-1.83E-04	4.97E-05	1.83E-04	-3.05E-05	5.15E-05
		24	-2.94E-04	3.80E-05	2.94E-04	-1.94E-05	3.87E-05
Y	x	8	-1.42E-05	6.93E-05	6.93E-05	5.19E-06	1.06E-05
		16	-2.55E-05	5.68E-05	5.68E-05	7.60E-06	1.56E-05
		24	-1.16E-05	6.22E-05	6.22E-05	4.84E-06	9.99E-06
	y	8	-0.607	0.216	0.607	-0.040	0.105
		16	-0.483	0.242	0.483	-0.059	0.139
		24	-0.521	0.121	0.521	-0.038	0.089
	z	8	-1.61E-03	9.32E-04	1.61E-03	-1.57E-04	4.34E-04
		16	-2.23E-03	1.39E-03	2.23E-03	-2.31E-04	7.11E-04
		24	-1.69E-03	8.63E-04	1.69E-03	-1.49E-04	4.86E-04

* Unit : ㎛

Other responses of the image motion on the x-axis and y-axis are summarized in Table 1. As shown in table 1, all the magnitudes of the image motion are less than 9 ㎛, the limit of the image motion. These results indicate that the design of the wide field telescope structure is relatively stiff enough to accommodate the operational wind condition for the image motion.

4. CONCLUSION

The image motion analyses of the wide field telescope were computed from the dynamic responses by using the LOS image sensitivity integrated in the finite element analysis method. It is fact that the LOS combined with the image motion is a useful and essential method to predict the opto-mechanical performance of the telescope. The results of the dynamic response based on the excitation load from the recorded wind velocity indicate that the wide field telescope system design requirement was satisfactorily fulfilled by maintaining the image motion of less than 9 ㎛ during the environment wind excitation.

5. REFERENCES

[1] ProLine PL16803 LDR CCD manual.

[2] E. Huang, Gemini Report, TN-O-G0017 (1992).

[3] J. H. Burge, “An easy way to relate optical element motion to system pointing stability,” Proc. SPIE, 6288, 62880I-1 (2006).

[4] M. K. Cho, NIO Report, RPT-GSMT-004 (2001).

[5] M. Johns, Optical Sensitivity Equations for use in the Dynamical Response Analysis for the Giant Magellan Telescope, Document 1114, GMT (2005).

[6] M. K. Cho, L. Stepp, and S. Kim, “Wind buffeting effects on the Gemini 8-m primary mirrors,” in Optomechanical Design and Engineering 2001, A. E. Hatheway, ed., Proc. SPIE 4444, 302-314 (2001).

[7] M. K. Cho, L. M. Stepp, G. Z. Angeli, and D. R. Smith, “Wind loading of large telescope,” in Large Ground-Based Telescopes, J.M. Oschman and L. M. Stepp, eds., Proc. SPIE 4837, 352-367 (2002).

[8] G. Z. Angeli, M. K. Cho, M. Sheehan, and L. M. Stepp, “Characterization of wind loading f telescope,” in Integrated Modeling of Telescopes, T. Anderson, ed., Proc. SPIE 4757, 72-83 (2002).